Available online at www.sciencedirect.com
SCIENCE DIRECT®
Journal of Power Sources 124 (2003) 390–402
JOURNAL OF POWER SOURCES
www.elsevier.com/locate/jpowsour

Issues on development of (La,Sr)MnO_3 cathode for solid oxide fuel cells

S.P. Jiang*

Fuel Cells Strategic Research Program, School of Mechanical and Production Engineering, Nanyang Technological University, Nanyang Avenue, Singapore 639798, Singapore

Abstract

Development of high-performance electrode materials is critical to the commercial realization of solid oxide fuel-cell (SOFC) technology. The material development process is, however, very complex and requires understanding of the fundamental issues of the materials and the electrochemistry that is involved. An interesting example is the (La,Sr)MnO_3 (LSM) cathode material. This paper discusses some important issues in the development and optimization of LSM cathode materials for SOFCs. The relationship between the microstructure, interfacial properties and the electrochemical behaviour of the cathode material is not a static one. Rather, it changes and evolves constantly under fuel-cell operation conditions. Such dynamic relationship between the properties and the electrochemical behaviour is important for the fundamental understanding of the mechanism and kinetics of the oxygen reduction at LSM cathodes, and for the development of high-performance cathodes for SOFCs that operate at intermediate temperatures (600–800 °C).

Keywords: LSM; Cathode; Solid oxide fuel-cell; Microstructure; Interface; Electrode behaviour

1. Introduction

Development of cathode materials with high electrochemical performance and long-term stability becomes an increasingly urgent task in the race to develop commercially viable solid oxide fuel cell (SOFC) technology which can operate at intermediate temperatures of 600–800 °C. This is because the overpotential losses for the O_2 reduction reaction on the cathode side are relatively high in SOFCs that use thin-film electrolyte technologies [1–4]. Among the cathode materials reported, (La,Sr)MnO_3 (LSM) based perovskites, due to their high stability and high electrocatalytic activity for oxygen reduction at high temperatures, are the most extensively studied and investigated materials for O_2 reduction [5–12]. Despite significant efforts, however, fundamental questions on the mechanism and kinetics of the O_2 reduction reaction and on the electrode behaviour of LSM materials under fuel-cell operation conditions still remain.

There is a general consensus that O_2 reduction on LSM electrodes is most likely controlled by surface processes, such as the oxygen dissociative adsorption process [13,14], gas-phase O_2 diffusion [15,16], and oxygen diffusion on the LSM surface [9,17–19]. It is well known that LSM is a predominant electronic conductor with negligible oxygen ion conductivity [20,21]. On the other hand, Brichzin et al. [22] studied the geometry dependence of cathode potential on a well-defined thin LSM microelectrode and found that the polarization resistance varied inversely with the area of the electrodes. This suggests that the rate-determining step of the reaction is related to the surface area of LSM or the LSM|electrolyte interface area. Kuznecov et al. [23,24] also proposed that the O_2 reduction is dominated by oxygen transport through the LSM bulk. The discrepancies that surround the electrode behaviour of LSM for O_2 reduction may be intrinsically linked to the variability in LSM electrode|Y_2O_3–ZrO_2 (YSZ) electrolyte interfacial contact, and to the significant polarization effect on the morphology and microstructure of the LSM materials. As pointed out by Mitterdorfer and Gauckler [25], the reaction of O_2 reduction at the LSM electrode is strongly affected by the formation of lanthanum zirconate at the three-phase boundary, and the formation of such a resistive lanthanum zirconate phase is closely related to the stoichiometric composition of LSM materials. Also, the polarization behaviour and morphology of the LSM electrodes are strongly affected by the cathodic-current-polarization treatment [9,26,27]. Depending on the conditions of the cathodic-current treatment, such as current density, temperature and polarization period, the impedance behaviour can be characterized with one to three arcs [9]. The morphology and microstructure of LSM

* Tel.: +65-6790-5010; fax: +65-6791-1859.
E-mail address: mspjiang@ntu.edu.sg (S.P. Jiang).

0378-7753/$ – see front matter © 2003 Elsevier B.V. All rights reserved.
doi:10.1016/S0378-7753(03)00814-0

electrode can also change under cathodic polarization potential [27]. In addition, manganese in the LSM perovskite structure is known to be mobile at high temperatures and under cathodic polarization potentials [25,28–31]. This could have significant effect on the interfacial properties of the LSM cathode and the YSZ electrolyte. This study presents some important material and electrochemical issues observed in the development of LSM cathode materials. The results demonstrate a dynamic and complex relationship between the electrode behaviour, the materials microstructure and the electrochemical polarization processes.

2. Experimental

The electrochemical performance of LSM cathodes is generally characterized by galvanostatic current interruption (GCI) and electrochemical impedance spectroscopy (EIS) techniques [32]. Electrolyte substrates have been prepared by isostatic pressing 8 mol% Y_2O_3–ZrO_2 powder (TZ8Y, Tosoh, Japan), followed by sintering at 1500 °C for 4 h in air. LSM powders with stoichiometric composition $(La_{0.80}Sr_{0.20})_{1.0}MnO_3$ (LSM-A) and non-stoichiometric composition $(La_{0.80}Sr_{0.20})_{0.90}MnO_3$ (LSM-B) were prepared by co-precipitation and solid-state reaction methods. For LSM powder prepared by the co-precipitation method, the powder was coarsened at 1000 °C for 4 h in air. For LSM powder prepared by the solid-state reaction method, the powders were coarsened at 1000 °C for 15 h, followed by sintering at 1050 °C for 20 h. The chemical composition of the LSM powder was analyzed by inductively coupled plasma-atomic emission spectrometry (ICP-AES). The phase composition of the LSM powders was identified by X-ray diffraction (XRD). The spectra for stoichiometric and non-stoichiometric LSM powders prepared by co-precipitation and solid-state reaction methods showed the perovskite phase only. LSM coatings were applied to electrolyte substrates by screen-printing, followed by firing at 1150 °C for 2 h. The electrode area was 0.5 cm^2. A three-electrode system was used for electrochemical measurements. Pt paste (Engelhard 6082) was painted on to the opposite side of the working electrode to make counter and reference electrodes. The counter electrode was positioned symmetrically to the working electrode, and a reference electrode was painted as a ring around the counter electrode.

The electrochemical performance of the LSM cathodes was also investigated in 50 mm × 50 mm YSZ electrolyte cells, in which Ni (50 vol.%)/TZ3Y (50 vol.%) cermet anodes were used. The reference electrodes were strip type (34 mm × 3 mm) and the gap between the electrode and the reference electrode was 5 mm. The electrode area was 11 cm^2. Pt and Ni woven meshes were used as current-collectors for the LSM cathodes and the Ni/TZ3Y cermet anodes, respectively. Information on the preparation of the electrode materials, the cell configuration and the electrochemical measurements in the development of LSM cathodes and Ni/TZ3Y cermet anodes are available elsewhere [8,9,33–35]. The microstructure of the LSM electrodes and the topography of the LSM/YSZ interface induced by polarization were studied by scanning electron microscopy (SEM, JEOL #5600LV, Quorum Technologies) and atomic force microscopy (AFM, Nanoscope IIIA, Digital Instruments). The LSM coating was removed by treatment with concentrated HCl acid before AFM examination.

To assess the contact resistance between the porous electrode coating and the current-collector, a four-probe technique was adopted in order to be compatible with the fuel-cell testing configuration. The test arrangement for both contact resistance and four-probe conductivity measurements is shown in Fig. 1. And 3 mol% Y_2O_3–ZrO_2 (TZ3Y, Tosoh, Japan) electrolyte plates were prepared by type-casting and fired at l500 °C. TZ3Y electrolyte substrates were 50 mm × 50 mm in dimension with a thickness of ~100 μm. A $La_{0.72}Sr_{0.18}MnO_3$ (LSM-B) coating was screen-printed on to the TZ3Y electrolyte and fired at 1150 °C. The dimension of the electrode coating was 34 mm × 34 mm and the thickness was around 50 μm. There was no anode coating on the other side of the electrolyte. The cell was open to air with an alumina felt to distribute the load evenly. The electrical contact for the current and voltage probes was made by Pt mesh which was along the 34 mm length of the LSM electrode coating and was 3 mm

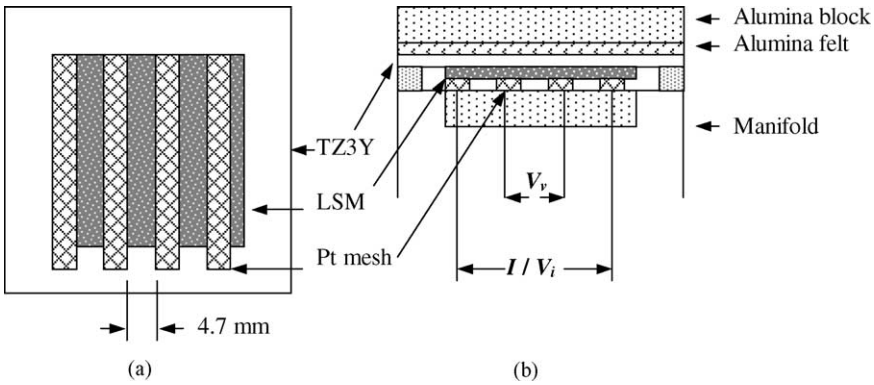

Fig. 1. Test cell (a) and test arrangement (b) for contact resistance and coating conductivity measurement.

in width. The average distance between the edges of the voltage probes was 4.7 mm. Measurement was carried out in air at 800 °C under various mechanical loads. Current was passed through the two outside meshes and the voltage was measured using the two inner meshes (voltage probes) and the two outer meshes (current probe). From the voltage measured by the voltage probes, the conductivity of the electrode coating was obtained using the formula

$$\sigma = \frac{I}{V_v}\frac{d}{lt} \quad (1)$$

where t is the thickness of the coating, l the length of the Pt mesh, d the distance between the Pt meshes, I and V_v are the applied current and voltage measured by the voltage probes, respectively. From the voltage measured by the current probe, the contact resistance can be estimated by subtraction of the resistance of the Pt wire and the LSM cathode coating.

$$R_{CR} = \frac{V_i}{I}A - R_{Pt} - R_{LSM} \quad (2)$$

where V_i is the voltage measured by the current probes, A the coating area between Pt current probes, R_{Pt} and R_{LSM} are resistance of the Pt wire and the LSM coating, respectively. The resistance of the Pt wire was measured separately and R_{LSM} was estimated from the conductivity of the coating, as determined by Eq. (1). Details of the test configuration are given in [36].

3. Results

3.1. Effect of powder morphology on coating microstructure

The first step in the development of Sr-doped $LaMnO_3$ (LSM) cathode materials is to synthesize LSM powder with the targetted composition and with controlled powder morphology in order to have a high degree of electrode performance reproducibility. The actual composition of the LSM powder depends, however, on the fabrication method. For LSM powder prepared by the solid-state reaction method, the final composition of LSM was found to be almost the same as the targetted composition. On the other hand, for LSM powder prepared by the co-precipitation method, the actual composition deviated slightly from the targetted one. For example, the actual compositions of LSM powder for stoichiometric and non-stoichiometric LSM compositions as determined by ICP-AES were $(La_{0.853}Sr_{0.147})_{0.98}MnO_3$ (A:B = 0.98) and $(La_{0.831}Sr_{0.169})_{0.89}MnO_3$ (A:B = 0.89), as compared with the targetted stoichiometric A:B = 1 composition of and a non-stoichiometric composition of A:B = 0.90. The deviation of the actual composition from that targetted may be related to the nature of the synthesis process, and therefore this possibility must be considered in the optimization of the LSM fabrication process.

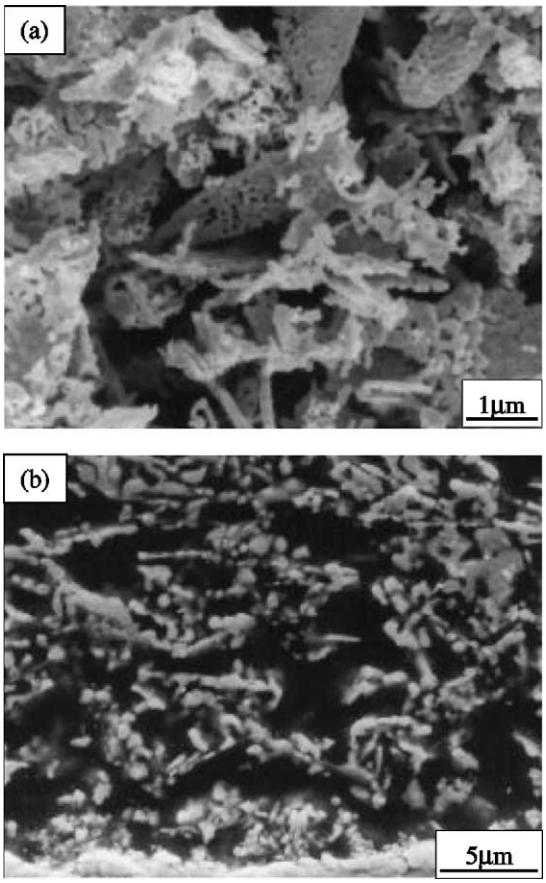

Fig. 2. Scanning electron micrographs of (a) $(La_{0.80}Sr_{0.20})_{0.90}MnO_3$ (LSM-B) power and (b) corresponding sintered electrode coating before fuel-cell testing. Powder prepared by co-precipitation method.

Control of the powder morphology is also important for optimization of the synthesis process of LSM powders. In the case of co-precipitation wet-chemical processing using starting materials of nitrate salts ($Sr(NO_3)_2$, $La(NO_3)_3$, $Mn(NO_3)_2$), the powder morphology is significantly affected by the processing parameters, such as precipitation conditions, washing procedure, and heating conditions in a static reactor or rotary reactor. Typical examples of the morphologies of a LSM-B powder and an electrode prepared by the co-precipitation method before fuel-cell testing are shown in Fig. 2. The size of the LSM-B particles is very small, namely ~0.1–1.2 μm. Fine LSM particles do, however, form large and flake-type agglomerates. Most important, the flake-type agglomerates of the powder still remain in the microstructure of the LSM electrode coating, to form a needle- or plate-like microstructure (Fig. 2b).The formation of such an anisotropic porous structure clearly originates from the geometric anisotropy of the LSM powder (see Fig. 2a). It has been shown that plate-like particles can be easily aligned perpendicular to the compression axis during uniaxial pressing, and thus induce the anisotropy of the powder packing structure [37,38]. The coating shrinkage varies significantly between 20 and 34%, which makes quality control of the

screen-printed coating more difficult. In fact, a LSM electrode with such an anisotropic porous structure shows poor performance reproducibility and high sensitivity to cell mechanical loading, as compared with electrodes that have isotropic particle-type morphology. This is consistent with a report [39] that Ni/YSZ cermet anodes with anisotropic microstructure have low electrical conductivity and poor performance. This indicates that the microstructure and polarization performance of LSM electrodes are strongly affected by the morphology of the powder. As the electrochemical activity of the LSM electrode is related closely to the electrode|electrolyte interface or so called three-phase boundary region [40–42], the ability to monitor and control the powder morphology is essential in scale-up of the electrode fabrication process for application in SOFCs.

3.2. Initial polarization behaviour and reversibility

It has been observed that freshly-prepared LSM electrodes show pronounced initial polarization behaviour with the cathodic or the anodic current, or with polarization treatment. The electrode impedance and polarization behaviour of a freshly-prepared $(La_{0.80}Sr_{0.20})_{0.90}MnO_3$ (LSM-B) electrode with cathodic current treatment at 200 mA cm^{-2} and 850 °C in air are given in Fig. 3. Before passing cathodic current, the impedance response is characterized by a small high frequency arc with a large and depressed arc at low frequencies. As shown previously [9], the initial impedance response of the LSM electrode can be characterized by an equivalent circuit with three (*RQ*) circuits in series (where *R* is the resistance and *Q* the constant phase element). With current passage, the impedance arcs are reduced significantly. A passage of cathodic current for only 5 min reduces the electrode polarization resistance (R_E) from 7.7 to ∼3.1 Ω cm^2, a reduction of 60%. The electrode impedance arc does not completely recover to the original size before the current passage treatment. Similar to the impedance behaviour, the polarization potential for the O_2 reduction reaction on the LSM electrode decreases rapidly with passage of cathodic current. As the change in the electrode ohmic resistance is small, the reduction in the cathodic potential ($E_{cathode}$) is primarily due to the reduction in the overpotential, η. The substantial reduction in both R_E and η indicates a significant activation effect of cathodic current treatment on the initial polarization

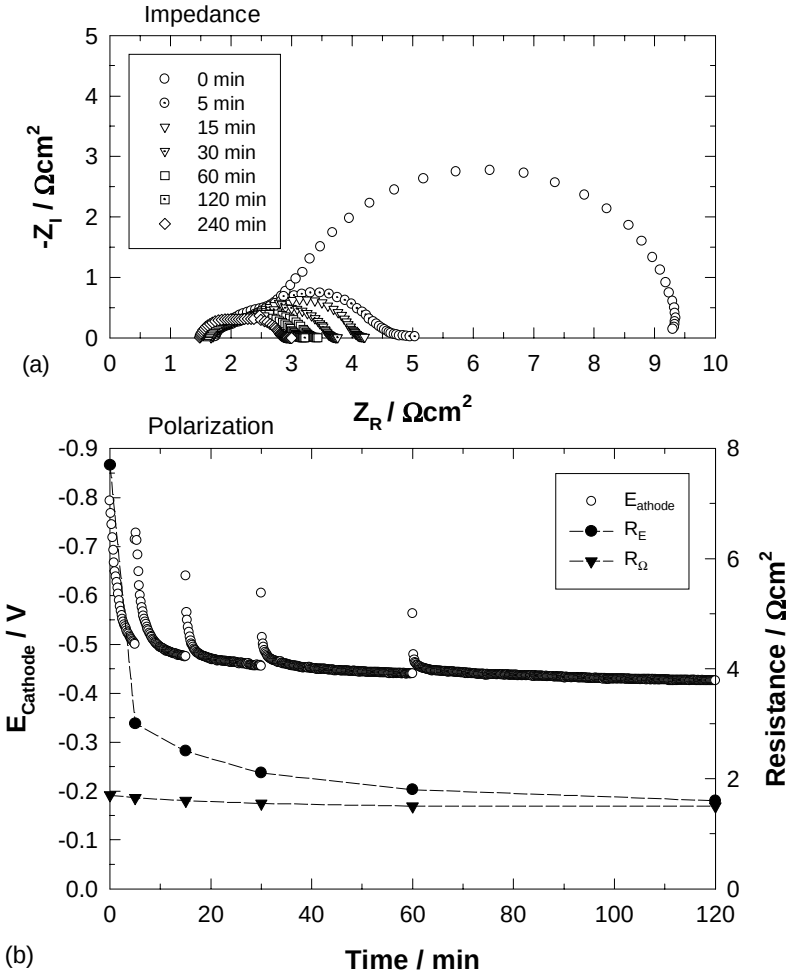

Fig. 3. Initial impedance (a) and polarization (b) behaviour of freshly-prepared $(La_{0.80}Sr_{0.20})_{0.90}MnO_3$ (LSM-B) electrode with cathodic current treatment at 200 mA cm^{-2} and 850 °C in air.

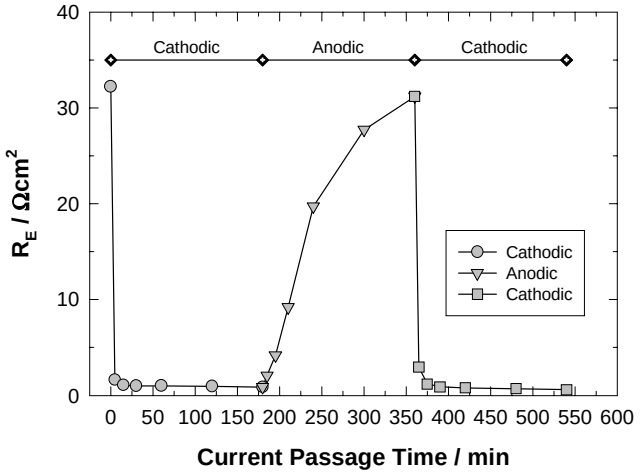

Fig. 4. Initial electrode polarization resistance of $(La_{0.80}Sr_{0.20})_{0.90}MnO_3$ (LSM-B) electrode as function of sequential cathodic, anodic and cathodic current treatment. Current treatment carried out at 100 mA cm^{-2} at 800 °C in air. R_E measured at open-circuit.

performance of the LSM electrode [9,26,43,44]. The activation effect of cathodic polarization has also been observed on LSM/YSZ composite electrodes [45,46]. Nevertheless, the extent of this effect is much smaller on LSM/YSZ composite electrodes than on pure LSM electrodes.

The electrode polarization resistance (R_E) of a LSM-B electrode is shown in Fig. 4 as a function of a sequential cathodic, anodic and cathodic current treatment. The current treatment was carried out at 100 mA cm^{-2} at 800 °C in air and R_E was measured by EIS at open-circuit. The initial polarization resistance before the cathodic current treatment was 32.2 Ω cm^2 After such treatment for 5 min, R_E was reduced to 1.64 Ω cm^2, i.e. ∼20 times smaller than the initial value. With the application of anodic polarization, the electrode polarization resistance increases monotonously with time. This is consistent with the observation of Tsukuda et al. [43]. The rate of increase in R_E with anodic polarization is much smaller than the rate of decrease in R_E in the case of cathodic current treatment. After 5 min of anodic current treatment, R_E increases to 2.1 Ω cm^2, only about two times higher than the R_E value before anodic current treatment (0.88 Ω cm^2). Only after prolonged anodic current treatment for 180 min, does R_E increase to 31.2 Ω cm^2, i.e. to almost the same value as the initial R_E of the freshly-prepared LSM electrode. Nevertheless, the activation effect of cathodic current treatment on the anodically polarized LSM electrode is almost identical to that on freshly-prepared LSM electrodes. The R_E is reduced from an initial value of 31.2–2.95 Ω cm^2 after cathodic polarization for only 5 min, i.e. ∼11 times smaller than the initial R_E.

The increase in R_E with the time of anodic current passage is an indication of the deactivation effect of the anodic polarization on the performance of the LSM cathode, in contrast to that of cathodic current polarization. This is supported by the fact that a change of polarization to cathodic direction again significantly decreases the electrode polarization resistance (Fig. 4). The reversibility of the electrode polarization behaviour of the LSM electrodes under anodic and cathodic current treatment indicates a significant mobility and diffusion of oxygen and cation species, such as Mn and Sr on the LSM surface [25,26,28–31,42,47]. According to Yokokawa et al. [48], oxygen plays an important role in the reductive dissolution of manganese from perovskite phase. Thus, the formation and accumulation of passivation species, such as SrO on the LSM surface and the re-combination of such species into the LSM perovskite structure could be closely related to the extent and direction of the polarization, and thus the oxygen partial pressure. The extraordinary deposition of Cr species on the zirconia electrolyte surface also demonstrates that cations, such as Mn are extremely mobile on the LSM surface under the influence of cathodic polarization in fuel-cell operation conditions [31,47].

3.3. Morphology and interface topography change induced by polarization

The significant mobility of oxygen vacancies and cation species on the LSM electrode surface under the influence of polarization is also indicated by the morphological change and reorientation of the LSM grains. Fig. 5 shows scanning electron micrographs of fractured cross-sections of a $(La_{0.8}Sr_{0.2})_{0.95}MnO_3$ (A:B = 0.95) electrode at the electrode|electrolyte interface before and after a cathodic current treatment of 500 mA cm^{-2} at 100 °C in air for 3 h. LSM electrode was sintered at 1100 °C in this case. The LSM electrode before the cathodic current treatment is characterized by a plate-like structure and each plate is an agglomerate of many small sphere-shaped particles.

After a cathodic current passage at 500 mA cm^{-2} and 1000 °C for 3 h, the morphology of the LSM grains is characterized by well-defined, granular-shaped particles. Tsukuda et al. [43] also observed the microstructural change of the contact points between the LSM grains and YSZ electrolyte. It was found that the change in the morphology of the electrode took place only in the interface region, the electrode bulk was unaffected.

AFM images of a YSZ electrolyte surface in contact with LSM-B electrodes after individual cathodic and anodic current treatment are presented in Fig. 6. Current treatment was performed at 100 mA cm^{-2} and 800 °C for 3 h in air, and the LSM electrode coating was removed by HCl treatment. A comparison of the YSZ surface without LSM contact and with LSM electrode contact but with no polarization is given in Fig. 6a and b. The contact topography between LSM particles and YSZ electrolyte is characterized by a ring which grows out of the YSZ electrolyte surface (Fig. 6b). Given that the LSM electrode used in this study is A-site non-stoichiometric, the formation of the ring is most likely due to the diffusion of manganese ions from LSM to YSZ during sintering of the LSM electrode coating, formation of lanthanum zirconate at the three-phase boundary is unlikely

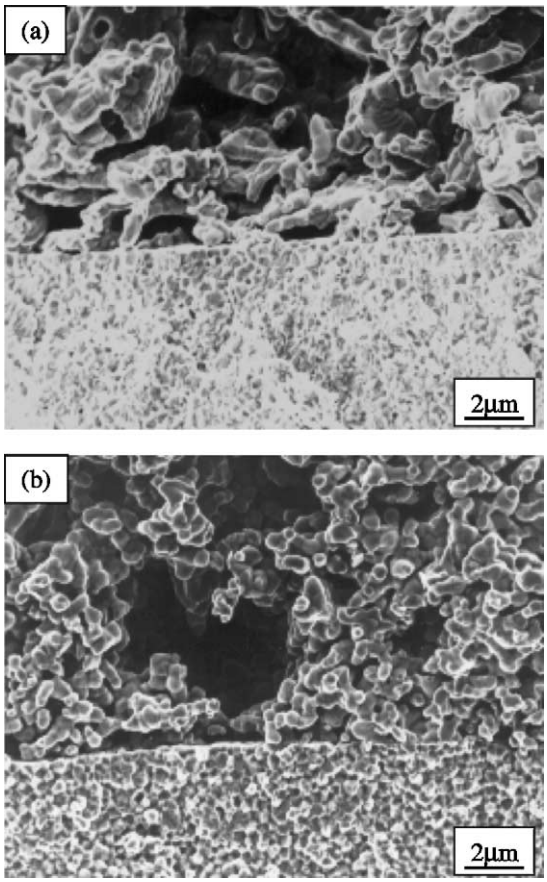

Fig. 5. Scanning electron micrographs of fractured cross-sections of $(La_{0.80}Sr_{0.20})_{0.95}MnO_3$ electrode at electrode|electrolyte interface region (a) before and (b) after cathodic current treatment of 500 mA cm^{-2} at 1000 °C in air for 3 h.

[25]. This is also indicated by the lack of formation of square islands which would indicate lanthanum zirconate on top of the rings. After cathodic current treatment of 100 mA cm^{-2} for 240 min at 800 °C, the sharp edge of the Mn–YSZ ring disappears and the ring grows outwards and broadens. This indicates that polarization not only induces a change in morphology and a reorientation of the LSM particles but also a morphological change at the LSM|YSZ interface (Fig 6c). Kuznecov et al. [24] also observed the formation of nanopores in the LSM|YSZ interface region after cathodic polarization treatment. The initial anodic current treatment affects the LSM/YSZ interface topography in a similar manner to cathodic current treatment, as shown in Fig. 6d. Nevertheless, no reaction layer is detected between the LSM and the YSZ electrolyte, as reported by Lee at al. [46] in a study of the formation of the reaction layer between a LSM|YSZ composite electrode and a YSZ electrolyte after anodic current passage of 1 A cm^{-2} at 900 °C for 24 h. This indicates that the initial LSM|YSZ interface is morphologically unstable. Either cathodic or anodic current treatment has a significant effect on the formation of the interface topography at the LSM|YSZ contact region. It is expected that such changes in topography will have an important influence on the electrochemical processes in the LSM electrode and YSZ electrolyte interface region.

The change in microstructure and polarization behaviour with cathodic polarization clearly indicates that the relationship between the microstructure and polarization performance is dynamic rather than static. The most significant change in the morphology at the interface that is induced by cathodic or anodic polarization occurs around the edge of the LSM particles in contact with YSZ electrolyte (i.e. the Mn–YSZ rings, as shown in Fig. 6). As manganese dissolution, diffusion and oxygen vacancy formation occur simultaneously on the LSM electrode surface under cathodic polarization [44], the change in the shape and the width of the rings indicates that the O_2 reduction reaction most likely occurs in Mn–YSZ ring region, i.e. in the three phase boundary region [5,25,40–42]. If the ring width is an indication of the width of the three-phase boundary, then the width of this boundary is about 0.25 μm which is similar in magnitude as that estimated by electrochemical and secondary-ion mass spectrometry (SIMS) measurements (<1 μm) [5,40,49]. Clearly, the relative magnitude of three-phase boundary (i.e. the ring area) and of the two-phase region between LSM grains and YSZ electrolyte would vary significantly with the LSM particle size and particle-size distribution, which may change with the polarization conditions. Such variation may offer some explanation of the discrepancies in the relation between the reaction rate, the three-phase boundary length and/or the two-phase contact areas [22–24,40,41,50].

3.4. Effect of contact and cell size on electrode performance

In addition to the effect of cathodic polarization on electrode behaviour, as described earlier, it has been found that the polarization performance of LSM electrodes is also dependent on the cell size. The performance of LSM cathodes and Ni/TZ3Y cermet anodes is shown in Fig. 7. The results were obtained on small button cells and on 50 mm × 50 mm plate cells at 900 °C in air and in 97% H_2/3% H_2O. The overpotentials were measured at 250 mA cm^{-2} and 900 °C. The effective electrode area of small coupon cells was 0.44 cm^2 and for 50 mm × 50 mm plate cells the effective electrode area was 10 cm^2. The small coupon cells and 50 mm × 50 mm plate cells were fabricated at the same time and used the same LSM and Ni/TZ3Y inks. The testing conditions were also similar for both types of cell. For Ni/TYZ3Y cermet anodes, there is a very good correlation between the performance measured on small coupon cells and on 50 mm × 50 mm cells. For LSM electrodes however, the performance measured on 50 mm × 50 mm plate cells is significantly lower than that measured on small button cells, in most cases. The size of the cell has a significant effect on the performance of LSM electrodes, but not on that of Ni/TZ3Y cermet anodes.

Electrical conductivity measurements on the porous electrode coatings show that the electrical conductivity of the porous Ni/TZ3Y cermet coating is ∼254 S cm^{-1}, which is

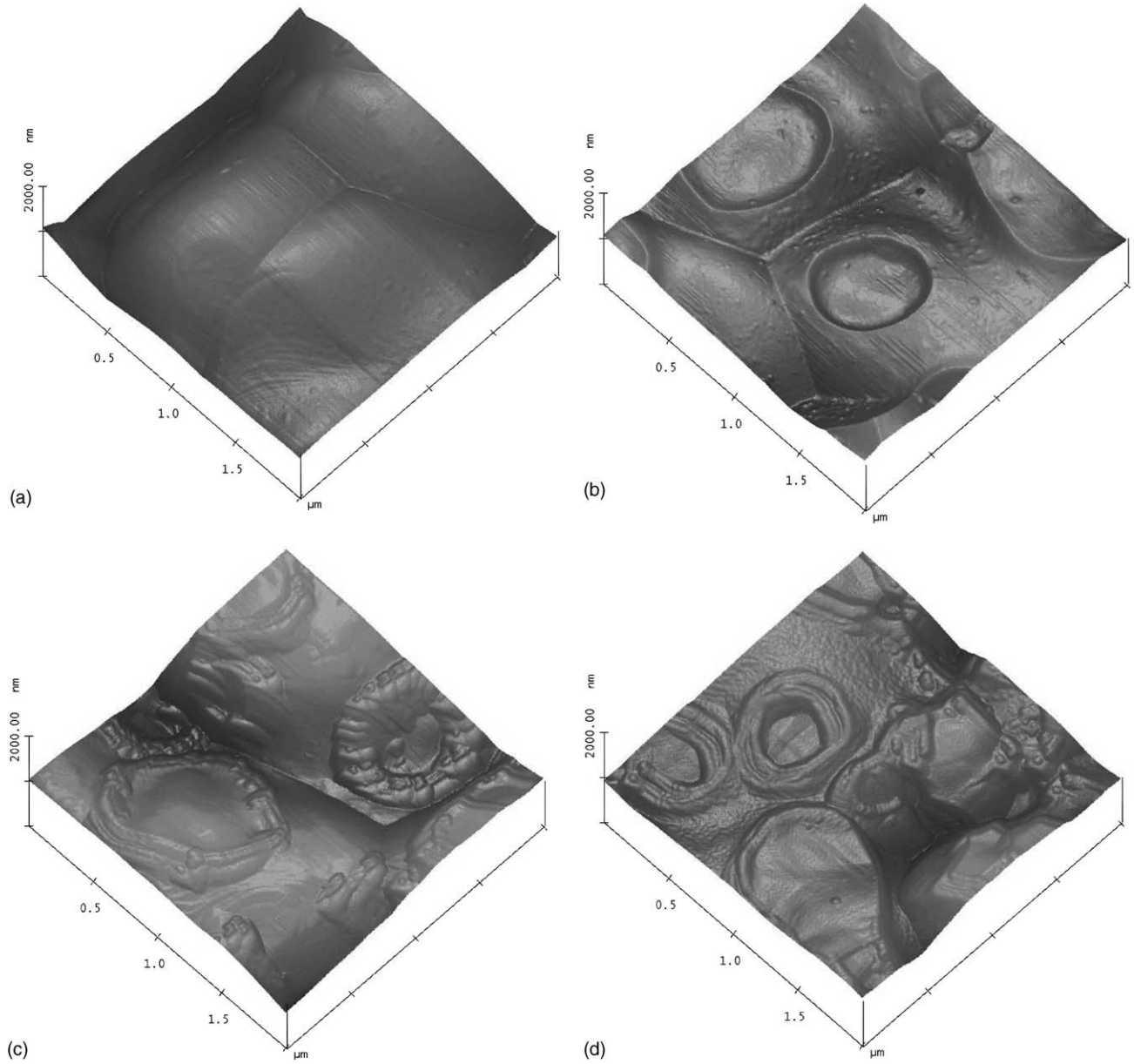

Fig. 6. AFM images of YSZ electrolyte surface: (a) without LSM electrode contact; (b) with LSM electrode and no polarization; (c) with LSM electrode after cathodic current treatment of 100 mA cm^{-2} at 800 °C for 180 min; (d) with LSM electrode after anodic current treatment of 100 mA cm^{-2} at 800 °C for 180 min. LSM electrodes were sintered at 1150 °C for 2 h in air.

much higher than 45 S cm^{-1} for the porous LSM electrode coating at 800 °C [36]. The much higher electronic conductivity of Ni/YSZ cermet anodes may be the reason for the decreased sensitivity of polarization performance with increase in cell size. It has been shown recently that the cell performance is dependent on the contact between the electrode coating and the current-collector [36]. High contact area is particularly important for an electrode coating with low electric conductivity. On the other hand, it has been found that the contact resistance between the Pt woven mesh current-collector and the LSM electrode coating depends on the operation temperature and the mechanical loading. The dependence of the contact resistance between a porous LSM electrode coating and a Pt woven mesh current-collector on mechanical loading measured at 800 °C is shown in Fig. 8. The empty symbols represent the measured results for two different samples of LSM electrode. The solid triangles are contact resistance of the LSM cathode side measured on 50 mm × 50 mm TZ3Y electrolyte cells, and the solid squares are the contact resistance of the LSM cathode side measured on 50 mm × 50 mm 9 mol% Sc_2O_3–ZrO_2 electrolyte cells at 800 °C. The contact resistances on 50 mm × 50 mm cells were measured between a conventional voltage probe and a special voltage probe on the same electrode side using a special cell configuration [51]. The results show that the contact resistance decreases significantly with increase

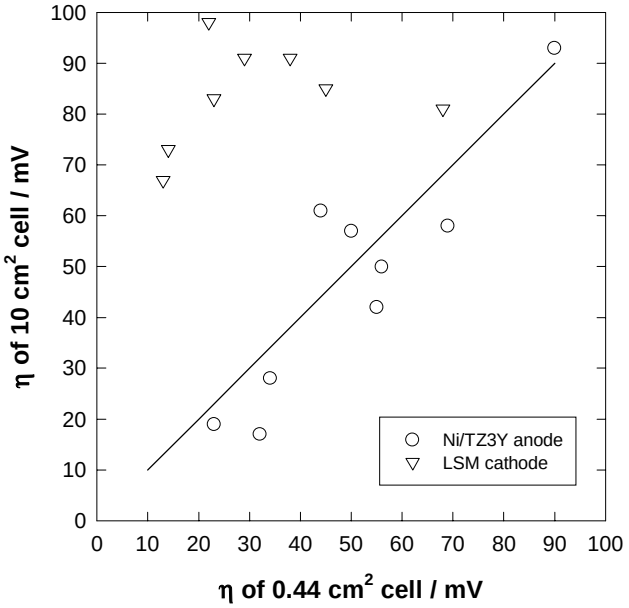

Fig. 7. Comparison of overpotentials of LSM cathodes and Ni/TZ3Y cermet anodes measured on small coupon cells (0.44 cm^2) and on 50 mm × 50 mm plate cells (10 cm^2) in air and in 97% H_2/3% H_2O, respectively. Overpotentials measured at 250 mA cm^{-2} and 900 °C.

in the mechanical loading. In general, the mechanical load on small button cells is due to the pressure applied by the spring and is generally about 1.5 kg cm^{-2} or higher, while for 50 mm × 50 mm TZ3Y electrolyte cells, the load is below 0.5 kg cm^{-2}. The mechanical load on the small button cell was several times higher than that on the 50 mm × 50 mm cell for the cells as described in Fig. 7. The difference in the mechanical loading on small button cells and on 50 mm × 50 mm cells results in a significant difference in the contact resistance. The high contact resistance will result in high polarization losses as the constriction effect not only occurs at the electrode|electrolyte interface, but also at the interface between the electrode and current-collector [36]. This explains the significant size effect on the polarization performance of porous LSM electrodes, as shown in Fig. 7.

The contact between the LSM electrode coating and the Pt current-collector also depends on the testing temperature. The Pt woven mesh current-collector used in this study is shown in Fig. 9 together with a LSM electrode contact surface after fuel-cell testing at 1000 °C under mechanical loading of 0.5 kg cm^{-2}. At an intermediate test temperature of 800 °C and a sample loading of 0.14 kg cm^{-2}, the contact between the Pt woven mesh and the LSM electrode would be mainly through the alternative cross-over; the rest of the mesh area is simply used to carry current laterally out of the system. In this case, the contact area of the Pt woven mesh current-collector with the LSM electrode coating is estimated to be ∼4.6%, and there is no clear contact mark of the Pt mesh on the LSM electrode coating [36]. In addition to the increased mechanical load to 0.5 kg cm^{-2}, increasing the test temperature to 1000 °C would have significant effect on the softening properties of Pt mesh. This is indicated by the clear mesh mark on the LSM electrode coating (Fig. 9c). From the contact marks, the contact area between the Pt woven mesh current-collector and the porous LSM electrode coating is estimated to be ∼56%, which is significantly higher than that of the designed contact area of the Pt mesh current-collector. Such an increase in the contact area would have a significant effect on the performance of LSM cathodes.

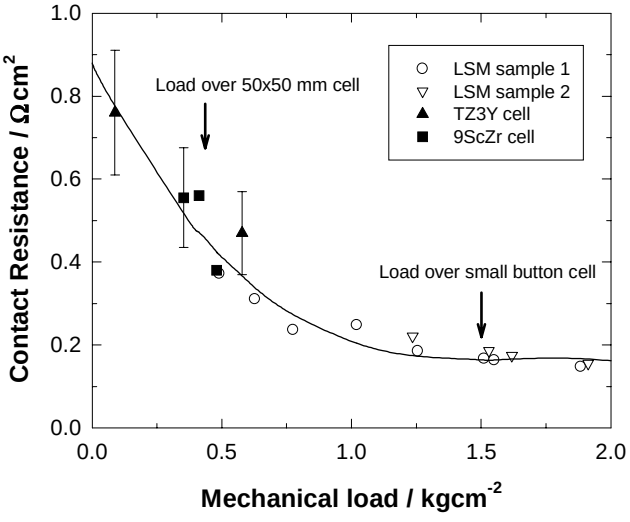

Fig. 8. Plots of contact resistance between LSM electrode coating and Pt mesh current-collector as function of mechanical load measured at 800 °C. See text for explanation of curves.

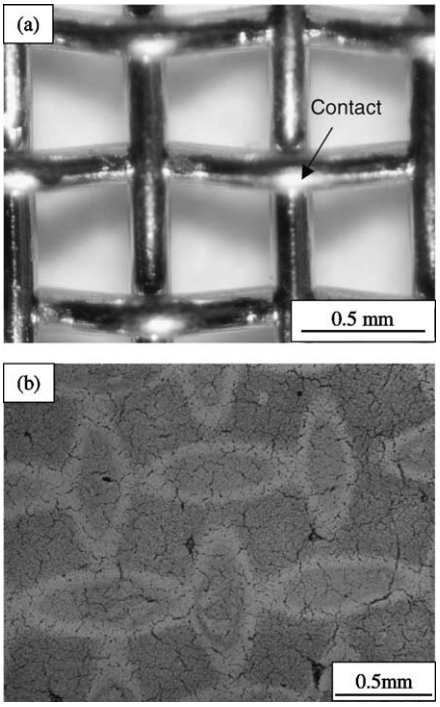

Fig. 9. Pt mesh current-collector (a) and LSM electrode surface (b), showing the Pt mesh contact marks after fuel-cell testing at 1000 °C.

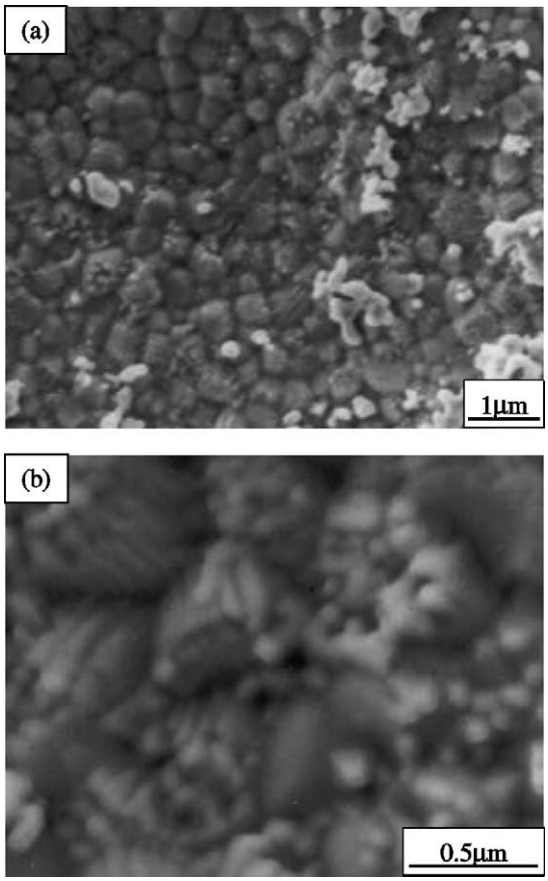

Fig. 10. Scanning electron micrographs of (a) TZ3Y electrolyte surface after removal of stoichiometric LSM electrode coating prepared by solid-state reaction method and (b) enlarged part of formation of columnar structure.

3.5. Interaction with other cell components

One of the most significant interactions between LSM electrodes and other cell components is the reaction with the YSZ electrolyte. The stability of LSM with YSZ electrolyte materials is related, however, to the stoichiometric composition of LSM. Yokokawa et al. [48] have shown that the significant A-site deficient lanthanum manganite inhibits the interfacial reaction with YSZ for the formation of lanthanum zirconate. In the case of LSM powders prepared by co-precipitation synthesis processes, non-stoichiometric LSM composition is essential to inhibit the formation of insulating pyrochlore zirconate phases at the LSM electrode and Y_2O_3–ZrO_2 electrolyte interface [8,9]. The same is also true for LSM powder prepared by the solid-state reaction method. Scanning electron micrographs of the TZ3Y electrolyte surface after removal of the stoichiometry $(L_{0.8}Sr_{0.2})_{1.0}MnO_3$ electrode coating are given in Fig. 10. The LSM electrode was prepared from stoichiometry LSM powder prepared by the solid-state reaction method and the electrode coating was fired at 1050 °C for 4 h in air. On the TZ3Y electrolyte surface in contact with the LSM electrode, the formation of small particles is clearly visible and the particles grow in a columnar structure. EDS identified the presence of Zr and La elements in these grains, which indicates the formation of a lanthanum zirconate phase on the TZ3Y electrolyte surface. This is consistent with the studies of Mitterdoft and Gauckler [25] on the dedicated relationship between the stoichiometric composition of LSM and the interface properties between LSM and YSZ [25]. A LSM electrode with stoichiometric composition shows low stability, low shelf-life, and poor electrode performance [8]. Thus, the non-stoichiometric composition (A-site deficiency) of LSM is important for LSM|YSZ interface stability and high-performance. A recent phase study [52] of the LSM–TZ3Y system showed that the fundamental reason for the beneficial effect of A-site deficient or Mn excess in LSM perovskite in inhibiting the formation of lanthanum zirconate is the fact that manganese oxide does not equilibrate with the lanthanum zirconate resistive phase, even though the LSM can be in equilibrium with either lanthanum or strontium zirconate phases at high temperatures [48].

With reduction of the operation temperature of a SOFC, metallic materials, such as Cr-based ferritic alloy and stainless steel can be used as the interconnect in place of doped $LaCrO_3$ ceramic [53–55]. Compared with ceramic materials, metallic interconnect materials are cheap, mechanically strong, much better in workability, and have high electrical conductivity and high heat conductivity. Chromium-based alloys, however, produce gaseous Cr species under the oxidizing environment and without an effective protective coating, the volatile Cr species can cause significant performance degradation of the LSM cathode [56–58]. Hilpert et al. [59] have demonstrated that thermodynamically, the electrochemical reduction of high valent Cr species to Cr_2O_3 can occur in competition with the O_2 reduction reaction under SOFC operating conditions. The electrochemical reduction of Cr species at the LSM|YSZ interface region in competition with O_2 reduction reaction is generally considered to be the deposition mechanism of Cr species under cathodic polarization conditions [56–58,60,61]. On the other hand, systematic studies on the deposition process of Cr species on LSM, Pt and (La,Sr) $(Co,Fe)O_3$ (LSCF) cathodes under different experimental conditions have provided convincing evidence that deposition of Cr species under SOFC operation conditions is not controlled by the electrochemical reduction of high valent Cr species in competition with O_2 reduction reactions in the electrode|electrolyte interface region. Rather, it is a chemical process in nature [31,47,62,63].

Scanning electron micrographs of LSM and Pt electrodes after passing cathodic current of 200 mA cm^{-2} at 900 °C in contact with Cr-based alloy for 4 and 22 h, respectively, are presented in Fig. 11. Details of the experimental set-up of the test cells can be found in [31,62]. For the LSM electrode, the coating was carefully removed to expose the YSZ electrolyte surface. LSM particles of irregular shape remained on the YSZ electrolyte surface. On the electrolyte surface between the LSM particles, there were fine grains (~0.05 μm) and relatively large crystals (~0.17 μm) (Fig. 11a). EDS

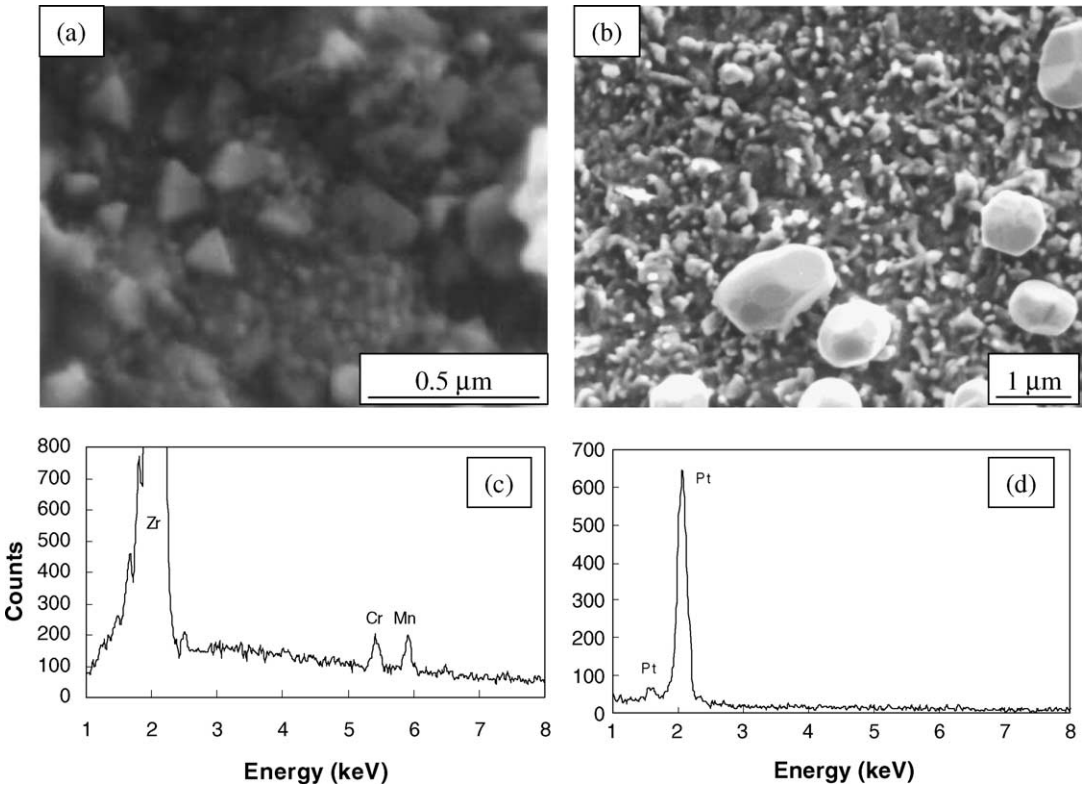

Fig. 11. Scanning electron micrographs of: (a) LSM electrode after cathodic current passage of 200 mA cm^{-2} at 900 °C for 4 h in contact with Cr-based alloy; (b) Pt electrode after cathodic current passage of 200 mA cm^{-2} at 900 °C for 22 h in contact with Cr-based alloy EDS pattern; (c) deposit particles on YSZ surface of LSM electrode; (d) deposit particles on YSZ surface of Pt electrode.

analysis showed that crystals contain Cr and Mn, which indicates that the crystals are most likely $(Cr,Mn)_3O_4$ spinel phase (Fig. 11c). Most importantly deposition of Cr species occurs not only on the areas close to the LSM|electrolyte interface, but also on the whole electrolyte surface between the LSM particles. The deposition of Cr species beyond the electrode|YSZ electrolyte region is also indicated by the formation of Cr deposit rings as wide as 300 μm on the YSZ electrolyte surface for the LSM electrode under polarization [47]. For the Pt electrode after polarization for 22 h in contact with the Cr alloy, there was no deposition of Cr species on either the YSZ electrolyte surface or on the Pt electrode surface (Fig. 11b). EDS analysis of large and small particles on the YSZ electrolyte surface shows the presence of Pt only (Fig. 11d). This suggests that deposition of Cr species at Pt electrodes is kinetically hindered as compared with that at LSM electrodes under cathodic polarization conditions. The fundamental reason for the significant dependence of the Cr deposition process on the nature of the electrode is that the driving force for Cr deposition under fuel-cell operating conditions is not the electrochemical polarization potential. In the case of a LSM cathode, the driving force for Cr deposition is most likely the Mn^{2+} species generated under cathodic polarization or at high temperatures [30,44]. For a $La_{0.6}Sr_{0.4}Co_{0.2}Fe_{0.8}O_3$ (LSCF) cathode, enrichment of SrO species on the surface is the main nucleation agent for the deposition of Cr species [62]. On the other hand, Pt is a poor nucleation agent for the deposition of gaseous Cr species. The results also indicate that in addition to the development of an effective and gas-tight protective layer for a Cr-based alloy interconnect, development of cathode materials which inhibit the formation of a nucleation agent could also be effective in the prevention of Cr deposition at the electrode.

In addition to the volatile Cr species from Cr-based metallic interconnect, gaseous species from other cell components can also be harmful to the performance of LSM cathodes. For example, volatile alkaline species, in particular Na_2O produced from borosilicate glass sealant containing Na and K at high temperatures, accelerate the grain growth of LSM particles and, thereby, leads to a decrease in the electrode polarization performance [64]. In general, the constituents in the cell components should have low volatility to minimize adverse effects on the performance and stability of the LSM electrode, or direct contact between the volatile species and the LSM electrode should be avoided through careful stack design.

3.6. Electrocatalytic effect under polarization

In addition to the activation effect of cathodic polarization on the initial electrode performance of the LSM cathode, as shown above, an electrocatalytic effect or enlargement of the reaction area on oxygen reduction could occur under cathodic polarization, as indicated by a significant

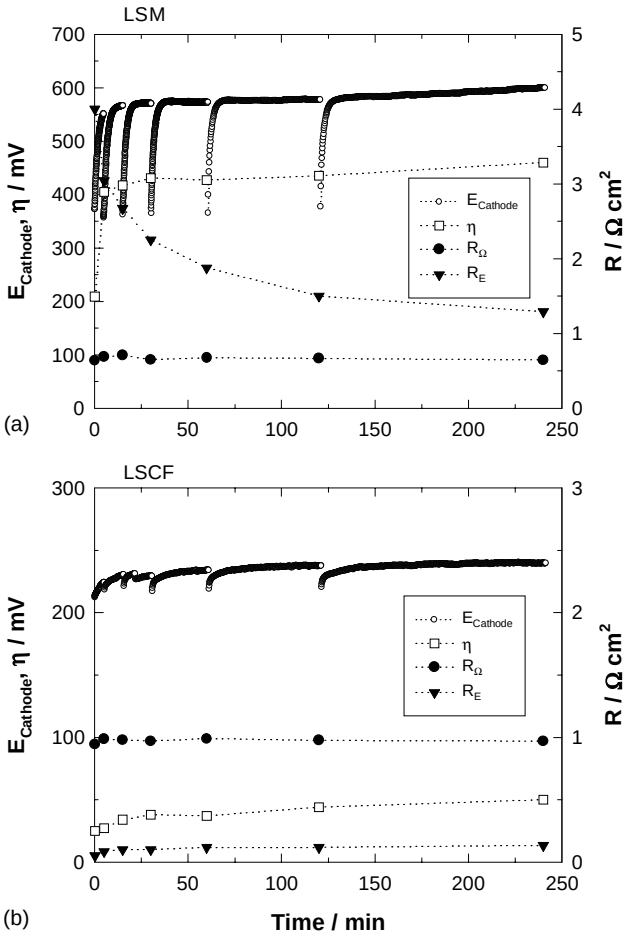

Fig. 12. Electrode behaviour of (a) $(La_{0.80}Sr_{0.20})_{0.90}MnO_3$ (LSM-B) and (b) $La_{0.6}Sr_{0.4}Co_{0.2}Fe_{0.8}O_3$ (LSCF) electrode under cathodic current of 200 mA cm^{-2} at 900 °C in air and in presence of gaseous Cr species.

decrease in electrode polarization resistance and an improvement in electrochemical performance [13,14,44,65]. There is, however, a diversity of opinion on whether LSM would develop a significant bulk diffusion property or ionic conductivity under cathodic polarization. Secondary-ion mass spectrometry (SIMS) studies on the LSM mesh electrode under polarization indicate that the oxygen diffusion through the LSM bulk is dependent on the polarization potential [5,49]. Under a cathodic overpotential of 0.336 V at 700 °C, oxygen ion was found to diffuse through LSM (∼0.5 μm thick) while at lower cathodic polarization, oxide ion did not diffuse through the LSM mesh. On the other hand, Kuznecov et al. [24] considered that the O_2 reduction reaction is dominated by oxygen diffusion through the LSM bulk. Recent findings of LSM electrode behaviour in the presence of chromium gaseous species offer some insight into the nature of O_2 reduction reaction under SOFC operation conditions [19,42,66].

The electrode behaviour of LSM and LSCF electrodes at a cathodic current of 200 mA cm^{-2} and 900 °C in air and in the presence of gaseous Cr species is shown in Fig. 12. The Cr gaseous species was introduced into the system by using a high Cr stainless-steel interconnect coupon in direct contact with the electrode [31]. The electrode polarization resistance (R_E) was measured by EIS at open-circuit. Characteristics of LSCF electrodes can be found in [19]. The change in polarization potential ($E_{cathode}$) for O_2 reduction on the LSM electrode with passage of cathodic current is opposite to that in the Cr species-free environment. Instead of a very rapid decreasing $E_{cathode}$ in the Cr species-free environment (see Fig. 3b), $E_{cathode}$ increased very rapidly with the cathodic current passage, and reached a potential plateau where the increase in $E_{cathode}$ was much slower. The change of $E_{cathode}$ with cathodic current passage was reproducible at the initial stage of the polarization. The instantaneous increase of $E_{cathode}$ and the almost complete reproducibility of the polarization behaviour with cathodic current passage indicate that the gaseous Cr species is a strong inhibitor of O_2 reduction reactions on LSM electrodes. Similar to that on LSM electrode, the polarization potential also increased with the passage of cathodic current on the LSCF electrode. The magnitude in the increase of $E_{cathode}$ is however smaller (Fig. 12b) This is most likely related to the high oxygen ion conductivity of the LSCF materials compared with that of LSM. LSM is a predominant electronic conductor with very low ionic conductivity (oxygen ion conductivity is $\sim 6 \times 10^{-7}$ S cm^{-1} at 900 °C [21]) while the oxygen ion conductivity of LSCF is much higher (∼0.2 S cm^{-1} at 900 °C [67]). The significant increase of polarization potential for O_2 reduction on the LSM electrode indicates that due to the presence of surface process inhibiting species, such as Cr gaseous species, the electrocatalytic effect of cathodic polarization is no longer effective despite the very high cathodic polarization potential (the cathodic potential can go as high as −0.98 V versus Pt air reference electrode at 900 °C and there is still no decrease in the overpotential for O_2 reduction on the LSM electrode [19]). This, in turn, shows that the oxygen vacancy cannot be initiated from the inside of the LSM electrode bulk under O_2 reduction polarization. Thus, the electrocatalytic effect due to oxygen vacancy formation observed on LSM electrodes under high polarization potentials is essentially a surface phenomenon in nature [19,66]. Even though the extent of the electrocatalytic effect of cathodic polarization on the O_2 reduction reaction on LSM electrodes cannot be quantified at this stage, it is most likely that such effect would be substantial and would probably be limited in the surface region.

4. Conclusions

The development of electrode materials for fuel cells is a complex process which involves examination and consideration of the material microstructure, interface properties and electrochemical process, in addition to optimization of the fabrication process. In the case of a LSM cathode, the material microstructure and interface properties are not

static but are constantly changing and evolving under polarization or fuel-cell operating conditions. It is important to optimize the fabrication process in order to achieve the optimum microstructure of the electrode. It is equally important to understand the dynamic relationship between the material properties, the interface properties at the electrode and electrolyte, the current-collector contact, and the electrochemical behaviour. These factors must be taken into account when determining and evaluating the mechanism and kinetics of the electrode reaction concerned. In addition to the factors discussed above, the thermal compatibility of the electrode material, together with the chemical stability and the tolerance of the electrode materials to the gaseous species produced by other fuel-cell components, such as interconnect and ceramic–glass sealant, should also be considered in the development of electrode materials for SOFCs.

References

[1] E. Ivers-Tiffée, A. Weber, D. Herbstritt, J. Eur. Ceram. Soc. 21 (2001) 1805.
[2] H. Yokokawa, N. Sakai, T. Horita, K. Yamaji, Fuel Cells 1 (2001) 117.
[3] B.C.H. Steele, Solid State Ionics 134 (2000) 3.
[4] O. Yamamoto, Electrochim. Acta 45 (2000) 2423.
[5] T. Horita, K. Yamaji, M. Ishikawa, N. Sakai, H. Yokokawa, T. Kawada, T. Kato, J. Electrochem. Soc. 145 (1998) 3196.
[6] J. Mizusaki, Y. Yonemura, H. Kamata, K. Ohyama, N. Mori, H. Takai, H. Tagawa, M. Dokiya, K. Naraya, T. Sasamoto, H. Inaba, T. Hashimoto, Solid State Ionics 132 (2000) 167.
[7] E.P. Murray, T. Tsai, S.A. Barnett, Solid State Ionics 110 (1998) 235.
[8] S.P. Jiang, J.P. Zhang, Y. Ramprakash, D. Milosevic, K. Wilshier, J. Mater. Sci. 35 (2000) 2735.
[9] S.P. Jiang, J.G. Love, J.P. Zhang, M. Hoang, Y. Ramprakash, A.E. Hughes, S.P.S. Badwal, Solid State Ionics 121 (1999) 1.
[10] F. Zheng, L.R. Pederson, J. Electrochem. Soc. 146 (1999) 2810.
[11] P. Decorse, G. Caboche, L.-C. Dufour, Solid State Ionics 117 (1999) 161.
[12] M.S. Islam, M. Cherry, L.J. Winch, J. Chem. Soc., Faraday Trans. 92 (1996) 479.
[13] B. Gharbage, T. Pagnier, A. Hammou, J. Electrochem. Soc. 141 (1994) 2118.
[14] E. Siebert, A. Hammouche, M. Kleitz, Electrochim. Acta 40 (1995) 1741.
[15] K. Tsuneyoshi, K. Mori, A. Sawata, J. Mizusaki, H. Tagawa, Solid State Ionics 35 (1989) 263.
[16] J. van Herle, A.J. McEvoy, K.R. Thampi, Electrochim. Acta 41 (1996) 1447.
[17] Y. Matsuzaki, I. Yasuda, Solid State Ionics 126 (1999) 307.
[18] M.J.L. Østergáard, M. Mogensen, Electrochim. Acta 40 (1995) 2015.
[19] S.P. Jiang, Solid State Ionics 146 (2002) 1.
[20] S. Carter, A. Selcuk, R.J. Chater, J. Kajda, J.A. Kilner, B.C.H. Steele, Solid State Ionics 53–56 (1992) 597.
[21] I. Yasuda, K. Ogasawara, M. Hishinuma, T. Kawada, M. Dokiya, Solid State Ionics 86–88 (1996) 1197.
[22] V. Brichzin, J. Fleig, H.-U. Habermeier, J. Maier, Electrochem. Solid State Lett. 3 (2000) 403.
[23] M. Kuznecov, P. Otschik, K. Eichler, W. Schaffrath, Ber. Bunseges. Phys. Chem. 102 (1998) 1410.
[24] M. Kuznecov, P. Otschik, P. Obenaus, K. Eichler, W. Schaffrath, Solid State Ionics 157 (2003) 371.
[25] A. Mitterdorfer, L.J. Gauckler, Solid State Ionics 111 (1998) 185.
[26] S.P. Jiang, J.G. Love, Solid State Ionics 138 (2001) 183.
[27] S.P. Jiang, J.G. Love, Solid State Ionics 158 (2003) 45.
[28] S.K. Lau, S.C. Singhal, Proc. Corros. 85 (1985) 79.
[29] D.M. Tricker, W.M. Stobbs, in: F.W. Poulsen, J.J. Bentzen, T. Jacobsen, E. Skou, M.J.L. Østergáard (Eds.), Proceedings of the 14th Risø International Symposium on Material Science, Risø National Laboratory, Roskilde, 1993, p. 453.
[30] D. Waller, J.D. Sirman, J.A. Kilner, in: U. Stimming, S.C. Singhal, H. Tagawa, W. Lehnert (Eds.), SOFC-V, The Electrochemical Society, Pennington, NJ, 1997, p. 1140.
[31] S.P. Jiang, J.P. Zhang, L. Apateanu, K. Foger, J. Electrochem. Soc. 147 (2000) 4013.
[32] S.P. Jiang, J.G. Love, S.P.S. Badwal, in: J. Nowotny, C.C. Sorrell (Eds.), Electrical Properties of Oxide Materials, Trans. Tech. Publications, Lancaster, 1997, p. 81.
[33] S.P. Jiang, Solid State Ionics, submitted for publication.
[34] S.P. Jiang, J.G. Love, Y. Ramprakash, J. Power Sources 110 (2002) 201.
[35] S.P. Jiang, P. Callus, S.P.S. Badwal, Solid State Ionics 132 (2000) 1.
[36] S.P. Jiang, J.G. Love, L. Apateanu, Solid State Ionics 160 (2003) 15.
[37] S. Gautier, E. Champion, D. Bernache-Assollant, J. Euro. Ceram. Soc. 17 (1997) 1361.
[38] A. Shui, Z. Kato, S. Tanaka, N. Uchida, K. Uematsu, J. Euro. Ceram. Soc. 22 (2002) 311.
[39] J.-H. Lee, J.-W. Heo, D.-S. Lee, J. Kim, G.-H. Kim, H.-W. Lee, H.S. Song, J.-H. Moon, Solid State Ionics 158 (2003) 225.
[40] F.H. van Heuveln, H.J.M. Bouwmeester, F.P.F. van Berkel, J. Electrochem. Soc. 144 (1997) 126.
[41] H. Fukunaga, M. Ihara, K. Sakaki, K. Yamada, Solid State Ionics 86–88 (1996) 1179.
[42] S.P. Jiang, J.P. Zhang, K. Foger, J. Electrochem. Soc. 147 (2000) 3195.
[43] H. Tsukuda, A. Yamashita, in: U. Bossel (Ed.), Proceedings of the First European Solid Oxide Fuel Cells Forum, European Fuel Cells Group, Lucerne, Switzerland, 1994, p. 715.
[44] H.Y. Lee, W.S. Cho, S.M. Oh, H.-D. Wiemhöfer, W. Göpel, J. Electrochem. Soc. 142 (1995) 2659.
[45] Y.J. Leng, S.H. Chan, K.A. Khor, S.P. Jiang, in: S.C. Singhal, M. Dokiya (Eds.), SOFC VIII, PV2003-07, The Electrochemical Society, Pennington, NJ, 2003, p. 440.
[46] Y.-K. Lee, J.-Y. Kim, Y.-K. Lee, I. Kim, H.-S. Moon, J.-W. Park, C.P. Jacobson, S.J. Visco, J. Power Sources 115 (2003) 219.
[47] S.P. Jiang, J.P. Zhang, K. Foger, J. Electrochem. Soc. 148 (2001) C447.
[48] H. Yokokawa, N. Sakai, T. Kawada, M. Dokiya, in: S.P.S. Badwal, M.J. Bannister, R.H.J. Hannink (Eds.), Science and Technology of Zirconia V, Technomic Publishing Co., Lancaster, 1993, p. 752.
[49] T. Horita, K. Yamaji, N. Sakai, H. Yokokawa, T. Kawada, T. Kato, Solid State Ionics 127 (2000) 55.
[50] J. Mizusaki, H. Tagawa, K. Tsuneyoshi, A. Sawata, J. Electrochem. Soc. 138 (1991) 1867.
[51] S.P. Jiang, J. Elctrochem. Soc. 148 (2001) A887.
[52] S.P. Jiang, J.-P. Zhang, K. Foger, J. Euro. Ceram. Soc. 23 (2003) 1865.
[53] E. Ivers-Tiffée, W. Wersing, M. Schiebl, H. Greiner, Ber. Bunsenges. Phys. Chem. 94 (1990) 978.
[54] S. Linderoth, P.V. Hendriksen, M. Mogensen, N. Langvad, J. Mater. Sci. 31 (1996) 5077.
[55] T. Brylewski, M. Nakoto, T. Maruyama, K. Przybylski, Solid State Ionics 143 (2001) 131.
[56] S. Taniguchi, M. Kadowaki, H. Kawamura, T. Yasuo, Y. Akiyama, Y. Miyake, T. Saitoh, J. Power Sources 55 (1995) 73.
[57] S.P.S. Badwal, R. Deller, K. Foger, Y. Ramprakash, J.P. Zhang, Solid State Ionics 99 (1997) 297.
[58] Y. Matsuzaki, I. Yasuda, Solid State Ionics 132 (2000) 271.
[59] K. Hilpert, D. Das, M. Miller, D.H. Peck, R. Wei, J. Electrochem. Soc. 143 (1996) 3642.

[60] Y. Matsuzaki, I. Yasuda, J. Electrochem. Soc. 148 (2001) A126.
[61] D. Das, M. Miller, H. Nickel, K. Hilpert, in: U. Bossel (Ed.), Proceedings of the First European SOFC Forum, European Fuel Cell Group, Lucerne, Switzerland, 1994, p. 703.
[62] S.P. Jiang, J.P. Zhang, X.G. Zheng, J. Euro. Ceram. Soc. 22 (2002) 361.
[63] S.P. Jiang, J.P. Zhang, L. Apateanu, K. Foger, Electrochem. Commun. 1 (1999) 394.
[64] S.P. Jiang, L. Christiansen, R. Hughan, K. Foger, J. Mater. Sci. Lett. 20 (2001) 695.
[65] Y. Jiang, S. Wang, Y. Zhang, J. Yan, W. Li, J. Electrochem. Soc. 145 (1998) 373.
[66] S.P. Jiang, J. Appl. Electrochem. 31 (2001) 181.
[67] Y. Teraoka, T. Nobunaga, K. Okamoto, M. Miura, N. Yamazoe, Solid State Ionics 48 (1991) 207.